Characterization of white poplar and eucalyptus after ionic liquid pretreatment as a function of biomass loading using x-ray diffraction and small angle neutron scattering

Xueming Yuan[a], Yonghao Duan[a], Lilin He[b], Seema Singh[c,d], Blake Simmons[c,e] and Gang Cheng[a,c,e*]

Abstract: A systematic study was performed to understand interactions among biomass loading during ionic liquid (IL) pretreatment, biomass type and biomass structures. White poplar and eucalyptus samples were pretreated using 1-ethyl-3-methylimidazolium acetate (EmimOAc) at 110°C for 3 hours at biomass loadings of 5, 10, 15, 20 and 25 wt.%. All of the samples were chemically characterized and tested for enzymatic hydrolysis. Physical structures including biomass crystallinity and porosity were measured by X-ray diffraction (XRD) and small angle neutron scattering (SANS), respectively. SANS detected pores of radii ranging from ~25 to 625 Å, enabling assessment of contributions of pores with different sizes to increased porosity after pretreatment. Contrasting dependences of sugar conversion on white poplar and eucalyptus as a function of biomass loading were observed and cellulose crystalline structure was found to play a more important role than porosity.

Keywords: Ionic liquid pretreatment; SANS; XRD; Biomass loading; Porosity

1. Introduction

Ionic Liquids (ILs) have been used to deconstruct lignocellulosic biomass for enhanced saccharification yield and rate, where the effectiveness of IL pretreatment is attributed to changes in cellulose crystalline structures (Cheng et al., 2011; Raj et al., 2016), accessibility of enzymes to cellulose (Torr et al., 2016) and lignin content (Pang et al., 2016; Raj et al., 2016). These three factors are coupled together which is determined by the compact and close association of cellulose, hemicellulose and lignin in plant cell walls (Keegstra, 2010). Previous studies of IL pretreatment have mainly focused on low biomass-to-IL ratio where biomass loading in ILs was less than 10 wt.% (da Silva et al., 2013). These studies are essential for the development of IL pretreatment techniques and form the foundation of more advanced processes being pursued (Xu et al., 2016).

Higher biomass loading is desirable during IL pretreatment since less amount og ILs is used. Yet, the number of studies which explored higher biomass loading is rather limited (Cruz et al., 2013; da Silva et al., 2013; Qiu et al., 2014; Wu et al., 2011). In 2011, Wu et al. conducted pretreatments at different biomass loadings of corn stover and found that the effectiveness of lowering biomass crystallinity index (CrI) decreased with increasing biomass loadings from 4.8 to 33 wt.% during pretreatments (Wu et al., 2011). The loss of lignin during pretreatments also showed similar trend, however delignification was not considered as necessary to improve sugar yield. Later, Cruz et al tested impact of biomass loading on IL pretreatment using switchgrass (Cruz et al., 2013). They found that cellulose II lattice was formed in switchgrass samples pretreated at biomass loadings of 3 to 30 wt.% and the biomass CrI decreased with increasing biomass loading. The cellulose in the sample pretreated at 50 wt.% loading became amorphous.

Lignin removal efficiency was also observed to decrease as the biomass loading was increased. da Silva et al used twin-screw extruder as a reactor to pretreat sugarcane bagasse in ILs, where pretreatments were conducted at biomass loadings of 11 to 50 wt.% (da Silva et al., 2013). Samples pretreated at 11-25 wt.% biomass loadings contained almost amorphous cellulose while only a small effect on the crystallinity obtained with the high solids loading of 50 wt%. No significant delignification was observed for all the samples. These studies suggest that pretreatment conditions and biomass types significantly affect the biomass structures and sugar conversion as a function of biomass loading.

The focus of this work was to provide a side-by-side comparison of physical structural changes of two hardwood biomasses that exhibited different response to IL pretreatment as a function of biomass loading. Two hardwood biomasses were chosen to minimize the variables involved. In this work, biomass samples were studied by XRD and SANS; covering a length scale of ~1 to 650 Å. Different biomass loadings caused contrasting changes to crystalline cellulose in white poplar and eucalyptus which might be due to differences in plant cell wall structures. For the first time, comparisons of porosity derived from SANS data were made and relative contributions from pores of different sizes to the porosity were evaluated for IL-pretreated biomass samples. The neutron scattering intensity is mainly coming from the contrast between pores and the biopolymers matrix; with the cellulose, hemicellulose and lignin phases have the scattering length density (SLD) of similar magnitude (Cheng et al., 2011). This highlights the unique capability of SANS on measuring biomass porosity and more work will be followed. Delignification was maintained roughly at the same level by varying amount

of anti-solvent used, allowing a clearer assessment of contributions of biomass CrI and porosity to sugar conversion.

2. Materials and Methods

2.1 Materials

Biomass samples were ground and sieved to retain particulates with sizes equal to or less than 2mm. Non-structural materials were extracted with a Soxhlet extractor using water and ethanol for 12h, respectively. The ionic liquid, EmimOAc, were purchased from Lanzhou Institute of Chemical Physics, China. Cellulase (NS50013, 137.3 mg protein/ml), β-glucosidase (NS50010, 208.7 mg protein/ml) and hemicellulose (NS22002, 21.5 mg protein/ml) were provided by Novozymes, China. The cellulose activity was measured to be 49 FPU/ml by the protocol of NREL (TP-510-42628, 1996).

2.2 Compositional analysis of white poplar and eucalyptus

Cellulose and hemicellulose contents were determined by a two-step acid hydrolysis and subsequent HPLC analysis, based on the standard NREL procedure (NREL/TP-510-42618). The sugar composition of the hydolysates was determined by high performance liquid chromatography (HPLC) using a refractive index detector (Hitachi, Tokyo, Japan). A Sugar-pak1 column (Waters, Milford, MA, USA) was used at 80^{o}C with ultrapure water as the eluent at a flow rate of 0.5mL/min. The lignin content was determined with the acetyl bromide method using an averaged extinction coefficient of 23.007 L g^{-1} cm^{-1} (Fukushima & Kerley, 2011).

2.3 Biomass pretreatment

Biomass solutions were prepared by combining 0.3g of biomass with varying amount of EmimOAc (5.7g, 2.7g, 1.7g, 1.2g and 0.9g to reach biomass loadings of 5, 10, 15, 20 and 25 wt.%) in 50 mL glass centrifuge tubes. The mixtures were heated in an oil bath without stirring at 110ºC for 3 h. Lower pretreatment temperatures such as 90 ºC did not cause much change to the cellulose crystalline structures of white poplar samples. In order to enable comparisons between white poplar and eucalyptus while keeping the temperature as low as possible, 110 ºC was found to be the right temperature. Stirring would certainly lead to faster mass and heat transport. Stirring is becoming difficult with biomass loading larger than 15 wt.% in EmimOAc (Li et al., 2013) unless special reactors are used, such as twin-screw extruder (da Silva et al., 2013). To be consistent, one did not stir the samples with different biomass loading, as was done by others (Cruz et al., 2013). An additional advantage of not stirring is saving energy.

After pretreatment, the reaction was quenched with different amount of water (34g, 37g, 38g, 38.5g and 38.8 g for samples of 5, 10, 15, 20 and 25 wt.%) and centrifuged or filtered. The amount of water added to the IL/biomass mixture was varied in such a way that the final weight of the water, IL and biomass was equal to 40 g. As will be explained later, varying amount of water was used to keep the lignin loss during pretreatments to roughly same level for all the pretreated samples. The pretreated biomass samples were then washed with same amount of water for 4 times. The recovered solids were lyophilized for 24h and then stored in a sealed plastic bag at 5ºC for analysis. For each pretreatment condition, three replicates were performed. The losses of biomass components, cellulose, hemicellulose and lignin, during pretreatment are calculated by the following equation:

Component loss = $1-\frac{\%\ \text{comonent in treated biomass} \times \%\ \text{recovered solids}}{\%\ \text{component in untreated biomass}}$ (1)

2.4 XRD measurement

The samples were scanned on a D8 ADVANCE diffractometer equipped with a sealed tube Cu Kα source. The operating voltage and current were 40 kV and 40mA and the x-ray wavelength was 0.15406nm. Scans were collected from 2θ = 5 to 60º with step size of 0.03 at 4 s per step. To minimize the uncertainty introduced by biomass pretreatment, samples obtained from 3 parallel pretreatments under the same condition were mixed for the XRD measurement. To ensure the reproducibility of the XRD data, microcrystalline cellulose (Avicel PH101) was measured each time along with other biomass samples.

2.5 SANS Measurement

The measurement was performed at the Oak Ridge National Laboratory (ORNL). Two sample–to-detector distances (SDDs) (1.7 and 14.5 m) with a detector offset of 40 cm and a neutron wavelength of λ=6 Å were used to cover scattering vectors ($q = \frac{4\pi\sin\theta}{\lambda}$, 2θ is the scattering angle) ranging from 0.004 to 0.4 $Å^{-1}$. Powder samples were loaded into quartz cells for the measurement. Since the bulk and skeleton density of the biomass particulates were not measured, the effective thickness was not available (Melnichenko, 2015), thus absolute calibration was not executed. However, a relative comparison of the scattering data was possible by normalizing the scattering curve by the mass of the sample put into the cell, assuming the particulates illuminated in the neutron beam have the similar packing density for different samples. The mass of the samples put into the cells was controlled to be around 70mg.

2.6 Enzymatic hydrolysis

Enzymatic hydrolysis of the samples was carried out in a reciprocating shaker (Scientific Industries, INC., SI-1402) at 50 °C and 30 rpm. All samples were diluted to 5 g substrates per liter in a 50 mM sodium acetate buffer with a pH of 4.8 supplemented with 0.08 g/L tetracycline. The total volume was 10 mL with cellulase (NS50013) concentration of 50 mg protein/g glucan, β-glucosidase (NS50010) concentration of 5 mg protein/g glucan and hemicellulase (NS22002) concentration of 34 mg protein/g xylan. The hydrolysate liquid after 24h hydrolysis was separated from the enzymatic residue by high speed centrifugation (10,000g for 10 min) and analyzed with DNS assay against a glucose standard. All assays were performed in triplicate.

3 Results and Discussion

The percentage of recovered solids as a function of biomass loading is shown in Figure 1a. It increases with increasing biomass loading for both white poplar and eucalyptus samples. This is attributed to decreased mass losses of cellulose and hemicellulose at higher biomass loadings, as shown in Figure 1 b and 1c. The sharp decrease in hemicellulose loss for white poplar sample at a biomass loading of 15 wt.% is due to experimental error. The general trend is that hemicellulose loss decreased with increasing biomass loading.It is interesting to notice that the mass loss of lignin, shown in Figure 1d, remains roughly the same as the biomass loading varies for both the pine and white poplar. Several prior studies have showed that lignin removal efficiency was observed to decrease as the biomass loading was increased (Cruz et al., 2013; Qiu et al., 2014; Wu et al., 2011). In this work, the amount of anti-solvent water added to the IL/biomass slurry at the end of pretreatment was not fixed to that of the IL used, i.e., it increased from ~6 to 40 times of IL with increasing of biomass loading. This is different

168 from the previous studies where the ratio of water to IL was either fixed (Qiu et al., 2014;
169 Wu et al., 2011) or varied slightly (Cruz et al., 2013). In a more recent study, it was found
170 that anti-solvent dosage affected lignin yield from eucalyptus globules wood treated with
171 IL-ethanol-water mixture (Liang et al., 2016). The amount of precipitated lignin first
172 increased with anti-solvent dosage that was followed by a decrease when the anti-solvent
173 dosage increased further (Liang et al., 2016). This might explain the observed lignin loss
174 in this work in that larger amount of water led to lesser lignin precipitation.

175 The most striking feature of biomass pretreatment using ILs is transformation of
176 cellulose crystalline structure via dissolution or swelling and regeneration (Cheng et al.,
177 2011; Cheng et al., 2015). Amorphous cellulose or cellulose II has lower recalcitrance
178 towards enzymatic hydrolysis than native cellulose. Figure S1a (Supporting Information)
179 presents the XRD data of white poplar samples after IL pretreatment. The XRD pattern of
180 untreated white polar sample is consistent with that of cellulose I lattice, indicated by the
181 presence of three peaks, a main peak at ~ 22°, a secondary peak at ~ 16° and a third small
182 peak at ~ 34.5° (Cheng et al., 2015). IL pretreatment leads to changes to cellulose
183 crystalline structure in the white poplar samples. The cellulose II structure, characterized
184 by the two peaks at ~ 12° and 20°, is present in the samples after pretreatment at biomass
185 loadings from 5 to 20 wt.%. The biomass CrI of cellulose II, extracted by a peak
186 deconvolution method (Zhang et al., 2015), decreases with increasing biomass loading:
187 0.44, 0.34, 0.31 and 0.27. This is consistent with the previous study (Cruz et al., 2013),
188 suggesting that higher cellulose to IL ratio leads to swelling instead of dissolution of
189 cellulose. It is believed that cellulose swollen by ILs leads to amorphous structure upon
190 regeneration in water (Zhang et al., 2014). The sample pretreated at a biomass loading of

25 wt.% contains a mixture of cellulose I (21.9° and 16.1°) and II lattice (12.2° and 19.9°), suggested by Figure S1b. Its overall biomass crystallinity index is 0.34.

On the other hand, the XRD data all of the pretreated eucalyptus samples have a pattern similar to that of cellulose I lattice, shown in Figure S1c. This suggests that eucalyptus samples are harder to get infiltrated by ILs. It is also consistent with the mass loss data. Eucalyptus samples have higher recovery percentages than those of white poplar samples, shown in Figure 1a. A closer look at the XRD data of pretreated eucalyptus samples indicates that the secondary peak at ~ 16° becomes broader. The full width at half maximums (FWHM), obtained by fitting the peak to a Gaussian function, are 6.1°, 6.8°, 6.7°, 6.1° for the samples pretreated at a biomass loading of 5, 10, 15 and 20 wt.%, respectively. An example of peak deconvolution is shown in Figure S1d. The FWHM is 2.8° for the untreated sample and 3.8° for the sample pretreated at a biomass loading of 25 wt.%. The secondary peak at ~ 16° contains diffractions from (110) and $(1\bar{1}0)$ planes (Cheng et al., 2015). Broadening of a diffraction peak indicates an increase of disorder between the corresponding crystallographic planes. The degree of distortion, indicated by the FWHM of the secondary peak, increases with biomass loading and reaches a maximum value at 15 wt.%. It then decreases with further increase of biomass loading.

It is interesting to note that a computer simulation work found that the cations of 1-butyl-3-methyl imidazolium chloride intercalated between (110) planes and $(1\bar{1}0)$ planes during cellulose dissolution. This should cause the broadening of the diffraction peaks. The peak positions are 15.4°, 15.1°, 14.9°, 14.5°, 14.1° and 14.9° for the untreated sample and pretreated samples at a biomass loading of 5, 10, 15 , 20 and 25wt.%,

respectively. This shift of the peak position to lower angle suggests an increase in the spacing between crystallographic planes, consistent with the cation intercalation. Meanwhile, the main peak position barely changes after pretreatment for all the samples and FWHM only increased from 2.4° to 2.8°. This suggests that the ordering of (200) plane is disturbed slightly. The above analysis shows that the (110) and $(1\bar{1}0)$ planes in cellulose I are the preferred interaction sites with IL molecules while the (200) plane is less favored one, consistent with prior studies (Yuan & Cheng, 2015).

Figure 2a presents the SANS data of untreated white poplar sample and the samples pretreated at biomass loadings of 5, 15 and 25 wt.%. The scattering curves follow power law over a q range from 0.1 to 0.004 $Å^{-1}$, which is similar to prior studies of biomass samples (Cheng et al., 2011). They also resemble the scattering data of other porous materials such as shale (Melnichenko, 2015; Ruppert et al., 2013). The power law scattering curves suggest a power law size distribution of pore sizes or fractal pore-matrix interface (Melnichenko, 2015). For polydisperse porous media, an appropriate relationship between pore radius (R) and the q is used: $R \approx 2.5/q$ (Melnichenko, 2015). Therefore SANS data in this work cover pores with radius in a range from ~ 25 to 625 Å. Increases in scattering intensity are observed for the samples after IL pretreatment, which indicates that the porosity is increased as a result of losses of biomass components during IL pretreatment. The relative contribution of pores with different sizes to the enhanced porosity is different. This is analyzed semi quantitatively by plotting the relative increase in scattering intensity at different q values, shown in Figure 2b. Three representative q values are chosen, corresponding to pores of radii of 63, 125 and 417Å. IL pretreatment results in creation of small pores compared to untreated sample, indicated by the

increased intensity around q=0.04 $Å^{-1}$ shown in Figure 2a. Smaller pores contribute less to the increased porosity than that from larger pores, as illustrated in Figure 2b. Figure 2c shows the SANS data of the eucalyptus samples. In contrast to white poplar samples, the magnitude of the intensity increase is smaller. This is consistent with mass loss data and XRD data which suggest that eucalyptus samples were difficult to be infiltrated by IL. Figure 2d presents the similar result as that of Figure 2b; smaller pores contribute to less to the increased porosity.

The SANS data were analyzed further by comparing the scattering invariant of different samples, $P = \frac{1}{2\pi^2}\int_0^\infty I(q)q^2\,dq$, representing the scattering power of a sample (Melnichenko, 2015). In this work, the scattering power is proportional to the concentration of pores or the porosity in the biomass samples. Since only a limited q rang was measured, the integration limit was from 0.004 to 0.1. The flat background from 0.1 to 0.4 $Å^{-1}$, arising from incoherent scattering, was subtracted from the SANS data before calculating the scattering power. Since the SANS data were not on an absolute scale, one compares the relative change of the porosity measured by SANS in this q range. The relative increases in porosity for white poplar samples, obtained by normalizing the scattering invariant of the pretreatment samples with that of untreated ones, after pretreatment are 2.9, 2.7 and 1.4 for biomass loadings of 5, 15 and 25 wt.%, respectively. They are 1.4, 1.5 and 1.3 for eucalyptus samples after pretreatment at biomass loadings of 5, 15 and 25 wt.%, respectively. The variation of relative increase of porosity is roughly consistent with mass loss data of cellulose and hemicellulose where more mass loss led to higher porosity.

Figure 3 shows the total sugar conversion after 24h of the biomass samples. It is interesting to notice that the sugar conversion increases with biomass loading for white poplar samples. This result correlates well with cellulose crystalline structure in the biomass samples. The sugar conversion increases with a drop in crystallinity index of cellulose II (Figure 3, right axis). The decrease in sugar conversion of the sample pretreated at a biomass loading of 25 wt.% is due to presence of cellulose I in that sample, which also increased overall biomass CrI. Relative changes in porosity also correlate with the sugar conversion, where higher porosity leads to better sugar conversion.

In contrast, the sugar conversion decreases with increasing biomass loading for eucalyptus samples. Since pretreated eucalyptus samples contain distorted cellulose I structure with varying degree of distortion, the biomass CrI is evaluated by comparing the ratio of the peak intensities at 18° and 22° (Cheng et al., 2011). The values of biomass CrI are 0.32, 0.35, 0.34, 0.36 and 0.42 for the samples pretreated at a biomass loading of 5, 10, 15, 20 and 25 wt.%, respectively. The CrI roughly correlates with sugar conversion (Figure 3, right axis) while the porosity does not; this suggests that the cellulose crystalline structure plays a more important role in sugar conversion.

4. Conclusion

Sugar conversion of pretreated white poplar samples increases with biomass loadings while it decreases for eucalyptus samples. This is correlated with changes in cellulose crystalline structure of biomass samples. XRD data indicate that native cellulose crystalline structure of eucalyptus sample was distorted, possibly due to intercalation of IL molecules between (110) planes and $(1\bar{1}0)$ planes. SANS data show that smaller pores

contributed less to the increased porosity than larger pores after IL pretreatment. The results obtained demonstrate different responses of white poplar and eucalyptus to IL pretreatment at different biomass loadings, offer further insights into IL pretreatment processes.

Acknowledgment

Gang Cheng acknowledges support for this research by the National Natural Science Foundation of China (U1432109) and China Scholarship Council (201606885004). We acknowledge support by the DOE Joint BioEnergy Institute (http:// www.jbei.org) through the U. S. Department of Energy, Office of Science, Office of Biological and Environmental Research, through contract DE-AC02-05CH11231 between Lawrence Berkeley National Laboratory and the U. S. Department of Energy. A portion of this research used resources at the High Flux Isotope Reactor, a DOE Office of Science User Facility operated by the Oak Ridge National Laboratory.

References:

1.Cheng, G., Varanasi, P., Li, C., Liu, H., Melnichenko, Y.B., Simmons, B.A., Kent, M.S., Singh, S. 2011. Transition of Cellulose Crystalline Structure and Surface Morphology of Biomass as a Function of Ionic Liquid Pretreatment and Its Relation to Enzymatic Hydrolysis. Biomacromolecules, 12, 933-941.

Cheng, G., Zhang, X., Simmons, B., Singh, S. 2015. Theory, practice and prospects of X-ray and neutron scattering for lignocellulosic biomass characterization: towards understanding biomass pretreatment. Energy Environ. Sci., 8, 436-455.

Cruz, A.G., Scullin, C., Mu, C., Cheng, G., Stavila, V., Varanasi, P., Xu, D., Mentel, J., Chuang, Y.-D., Simmons, B.A., Singh, S. 2013. Impact of high biomass loading on ionic liquid pretreatment. Biotechnol. Biofuels, 6.

da Silva, A.S.A., Teixeira, R.S.S., Endo, T., Bon, E.P.S., Lee, S.-H. 2013. Continuous pretreatment of sugarcane bagasse at high loading in an ionic liquid using a twin-screw extruder. Green Chem., 15, 1991-2001.

Fukushima, R.S., Kerley, M.S. 2011. Use of Lignin Extracted from Different Plant Sources as Standards in the Spectrophotometric Acetyl Bromide Lignin Method. Journal of Agricultural and Food Chemistry, 59, 3505-3509.

Keegstra, K. 2010. Plant Cell Walls. Plant Physiol., 154, 483-486.

Li, C., Tanjore, D., He, W., Wong, J., Gardner, J.L., Sale, K.L., Simmons, B.A., Singh, S. 2013. Scale-up and evaluation of high solid ionic liquid pretreatment and enzymatic hydrolysis of switchgrass. Biotechnol. Biofuels, 6, 154.

Liang, X., Liu, J., Fu, Y., Chang, J. 2016. Influence of anti-solvents on lignin fractionation of eucalyptus globulus via green solvent system pretreatment. Sep. Purif. Technol., 163, 258-266.

Melnichenko, Y.B. 2015. *Small-Angle Scattering from Confined and Interfacial Fluids: Applications to Energy Storage and Environmental Science*. Springer International Publishing.

Pang, Z.Q., Lyu, W.K., Dong, C.H., Li, H.X., Yang, G.H. 2016. High selective delignification using oxidative ionic liquid pretreatment at mild conditions for efficient enzymatic hydrolysis of lignocellulose. Bioresour. Technol., 214, 96-101.

Qiu, Z., Aita, G.M., Mahalaxmi, S. 2014. Optimization by response surface methodology of processing conditions for the ionic liquid pretreatment of energy cane bagasse. J. Chem. Technol. Biotechnol., 89, 682-689.

Raj, T., Gaur, R., Dixit, P., Gupta, R.P., Kagdiyal, V., Kumar, R., Tuli, D.K. 2016. Ionic liquid pretreatment of biomass for sugars production: Driving factors with a plausible mechanism for higher enzymatic digestibility. Carbohydr. Polym., 149, 369-381.

Ruppert, L.F., Sakurovs, R., Blach, T.P., He, L., Melnichenko, Y.B., Mildner, D.F.R., Alcantar-Lopez, L. 2013. A USANS/SANS Study of the Accessibility of Pores in the Barnett Shale to Methane and Water. Energy Fuels, 27, 772-779.

Torr, K.M., Love, K.T., Simmons, B.A., Hill, S.J. 2016. Structural features affecting the enzymatic digestibility of pine wood pretreated with ionic liquids. Biotechnol. Bioeng., 113, 540-549.

Wu, H., Mora-Pale, M., Miao, J., Doherty, T.V., Linhardt, R.J., Dordick, J.S. 2011. Facile pretreatment of lignocellulosic biomass at high loadings in room temperature ionic liquids. Biotechnol. Bioeng., 108, 2865-2875.

Xu, F., Sun, J., Konda, N., Shi, J., Dutta, T., Scown, C.D., Simmons, B.A., Singh, S. 2016. Transforming biomass conversion with ionic liquids: process intensification and the development of a high-gravity, one-pot process for the production of cellulosic ethanol. Energy Environ. Sci., 9, 1042-1049.

Yuan, X., Cheng, G. 2015. From cellulose fibrils to single chains: understanding cellulose dissolution in ionic liquids. PCCP, 17, 31592-31607.

Zhang, J., Wang, Y., Zhang, L., Zhang, R., Liu, G., Cheng, G. 2014. Understanding changes in cellulose crystalline structure of lignocellulosic biomass during ionic liquid pretreatment by XRD. Bioresour. Technol., 151, 402-405.

Zhang, J., Zhang, X., Li, C., Zhang, W., Zhang, J., Zhang, R., Yuan, Q., Liu, G., Cheng, G. 2015. A comparative study of enzymatic hydrolysis and thermal degradation of corn stover: understanding biomass pretreatment. RSC Adv., 5, 36999-37005.

Figure captions

Figure 1 Percentage of recovered solids as a function of biomass loading (a); Loss of cellulose (b), hemicellulose (c) and lignin (d) as a function of biomass loading.

Figure 2 SANS data of IL pretreated white poplar samples (a); relative increase in intensity at various q values for white poplar samples (b); SANS data of IL pretreated eucalyptus samples (c); relative increase in intensity at various q values for eucalyptus samples (d);

Figure 3 Total sugar conversion as a function of biomass loadings (left axis); Biomass CrI as a function of biomass loadings (right axis).

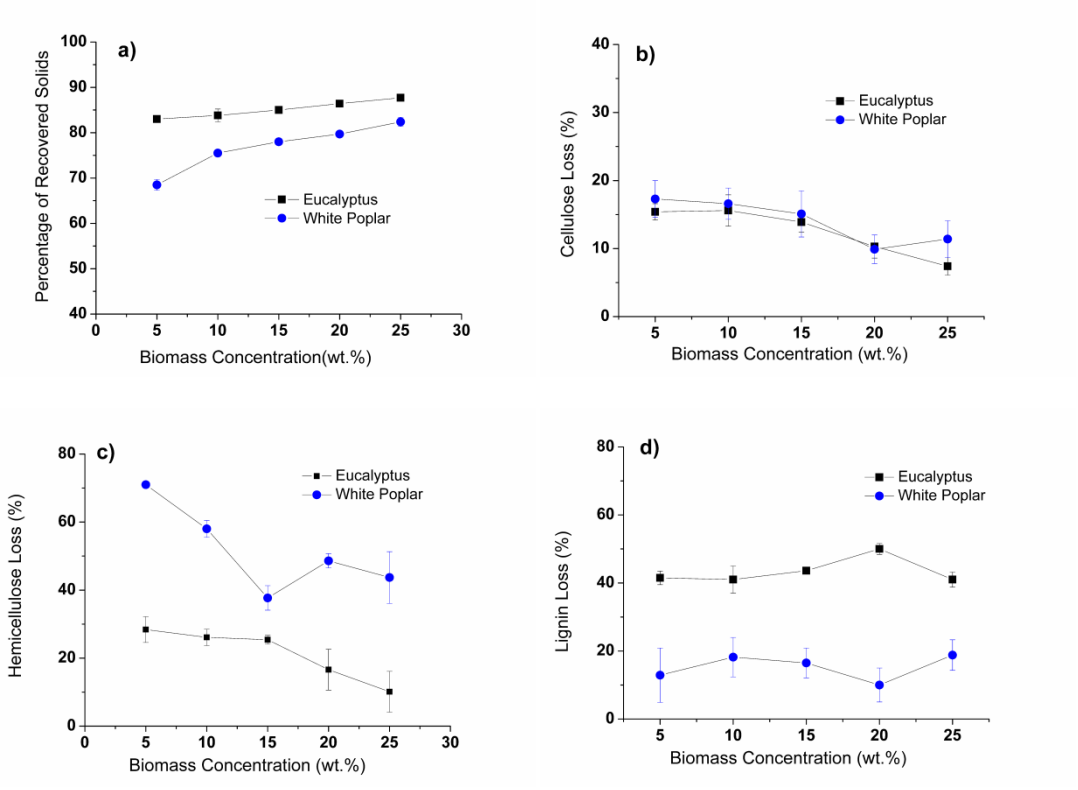
a)
Percentage of Recovered Solids
Biomass Concentration(wt.%)
Eucalyptus
White Poplar
b)
Cellulose Loss (%)
Biomass Concentration (wt.%)
Eucalyptus
White Poplar
c)
Hemicellulose Loss (%)
Biomass Concentration (wt.%)
Eucalyptus
White Poplar
d)
Lignin Loss (%)
Biomass Concentration (wt.%)
Eucalyptus
White Poplar

Figure 1

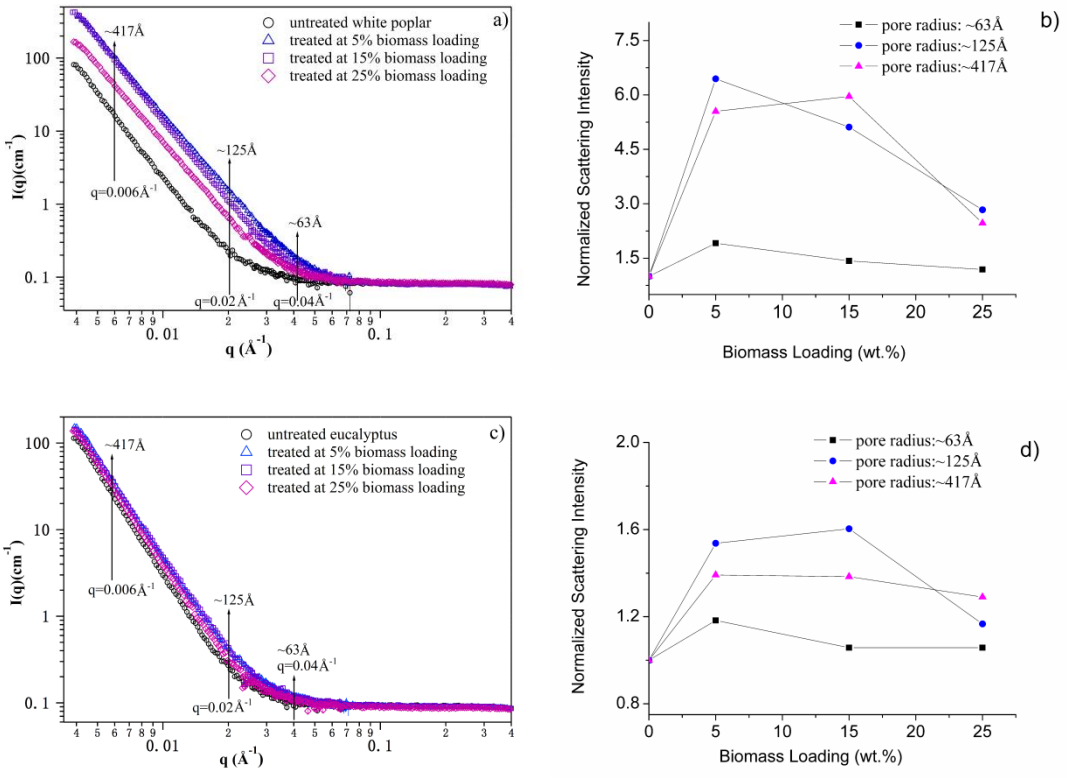
a)
untreated white poplar
treated at 5% biomass loading
treated at 15% biomass loading
treated at 25% biomass loading
~417Å
~125Å
~63Å
q=0.006Å⁻¹
q=0.02Å⁻¹
q=0.04Å⁻¹
I(q)(cm⁻¹)
q (Å⁻¹)
b)
pore radius: ~63Å
pore radius:~125Å
pore radius:~417Å
Normalized Scattering Intensity
Biomass Loading (wt.%)
c)
untreated eucalyptus
treated at 5% biomass loading
treated at 15% biomass loading
treated at 25% biomass loading
~417Å
~125Å
~63Å
q=0.006Å⁻¹
q=0.02Å⁻¹
q=0.04Å⁻¹
I(q)(cm⁻¹)
q (Å⁻¹)
d)
pore radius:~63Å
pore radius:~125Å
pore radius:~417Å
Normalized Scattering Intensity
Biomass Loading (wt.%)

Figure 2

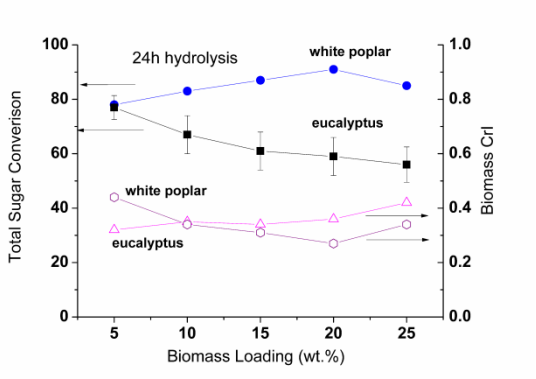
24h hydrolysis
white poplar
eucalyptus
white poplar
eucalyptus
Total Sugar Conversion
Biomass CrI
Biomass Loading (wt.%)
100
80
60
40
20
0
1.0
0.8
0.6
0.4
0.2
0.0
5
10
15
20
25

Figure 3